Hybrid NMR: A Union of Solution and Solid-State NMR

Pallavi Thiagarajan-Rosenkranz, Adrian W. Draney and Justin L. Lorieau[*]

Department of Chemistry, University of Illinois at Chicago, 845 W Taylor St, Chicago IL

60607

* Corresponding Author: justin@lorieau.com

ABSTRACT

Hybrid NMR (hdNMR) is a powerful new tool that combines the strengths of solution and solid-state NMR to measure dipolar, chemical shift and quadrupolar tensors in aqueous solution. We introduce the theory of hdNMR and partially randomly oriented (PRO) crystalline hydrogel samples. PRO samples produce randomly oriented spectra with characteristic Pake patterns from the solid-state, yet they maintain the high-resolution dispersion of solution NMR experiments. With new pulse sequences, we show how hdNMR can be used to measure with high precision the $^1H^\alpha$-$^{13}C^\alpha$ dipolar tensor and carboxylate chemical shift anisotropy tensor of aspartate. These measurements contain detailed information on the distribution of electron density, interatomic distances and the orientation dependence of molecular motion.

INTRODUCTION

Nuclear Magnetic Resonance (NMR) is one of most fruitful tools for studying the chemistry and biochemistry of molecules. The chemical shift, magnetic dipole-dipole (dipolar) interaction and quadrupolar interactions contain rich structural, dynamic and stereoelectronic information of atoms in molecules. A plethora of NMR techniques allow researchers to site-specifically measure torsional angles, internuclear distances, bond orientations and dynamics on a picosecond to seconds, and longer, timescale.[1] Both solution and solid-state NMR have useful and complementary advantages. In the solution state, molecules tumble rapidly and isotropically, producing high-resolution spectra amenable to detailed, site-specific studies on molecular structure, dynamics and function. The solid-state NMR experiment contains intricate orientation-dependent information from the anisotropic Hamiltonian, and it can be used to study samples that are not readily dissolved in solution or crystallized, such as amyloid fibrils.

Many important advances in solution and solid-state NMR have combined some of the advantages of each technique with the other. Solution NMR with liquid crystals, for instance, introduces weak partial alignment (PA) of molecules, yielding orientation information from residual dipolar couplings (RDC) and residual anisotropic chemical shifts (RACS) analogous to single crystals in the solid-state.[2] Solid state experiments that incorporate magic-angle spinning at very high speeds produce spectra with resolutions approaching those of the solution state, yet still retain the dipolar transfer mechanisms of solid-state NMR. In this report, we describe a new approach, named hybrid NMR (hdNMR), that extends the advantages of both techniques for soluble samples. Hybrid NMR experiments measure the anisotropic dipolar, chemical shift anisotropy (CSA) and quadrupolar tensors, conventionally available directly only from the solid-state spectrum, with the resolution and correlation information available from the solution state.

Our approach uses partially randomly oriented (PRO) crystalline hydrogel samples. We prepare crystalline hydrogel samples by affixing an aqueous nematic liquid crystal, pinacyanol acetate (PNA), in an agarose hydrogel matrix. The hydrogel prevents spontaneous uniaxial alignment of the liquid crystal in the magnetic field, and a spherical distribution consistent with a biaxial powder pattern is achieved. A similar procedure has been used to measure individual g-tensors by electron spin resonance (ESR) or quadrupolar tensors at individual sites[3,4] with partial disorder in the liquid crystal. The key differences in our approach are the development of a highly randomized crystal system, the use of an aqueous hydrogel compatible with high magnetic fields, and the production of spherical distributions that can still produce high-resolution spectra of biomolecules.

In the hdNMR experiment, molecules interact weakly with the crystals to produce Pake or powder-like spectra. Suppression of the anisotropic tensor lineshape can be achieved using conventional decoupling methods, and these tensors are readily correlated to high-resolution chemical shift dimensions using separated local field (SLF) pulse sequences.

In this report, we investigate the theory of hdNMR and its application to measuring anisotropic magnetic interaction tensors in a small molecule.

THEORY

The frequencies of magnetic interactions, including the chemical shift, dipolar, J-coupling, quadrupolar and other interactions, depend on the orientation of the interaction in the magnetic field, and they are represented by spatial tensors.[5] They can be expressed in a Cartesian basis or an irreducible spherical representation, which offers simplified rotational operations.[6] In the spherical representation, each spherical tensor consists of one 0th rank, isotropic component (V_{00}), three 1st rank anti-symmetric components (V_{1r}, with r=±1, 0) and five 2nd rank symmetric components (V_{2q}, with q=±2, ±1 and 0). The rank groupings are based on their rotational properties. Only the isotropic and symmetric components contribute to the NMR spectrum.[5] In the rotating frame, the non-secular components (r=±1, q=±2, ±1) in the truncated first order Hamiltonian are averaged to zero, and only the isotropic and the q=0 component of the symmetric tensor directly influences the frequencies of peaks in the spectrum. Consequently, the final observed frequency in the laboratory frame (LAB) measured for a given magnetic interaction depends on the sum of the isotropic ($V_{00}^{(LAB)}$) and the 2nd rank anisotropy ($V_{20}^{(LAB)}$) of the spatial tensor.

The 2nd rank tensors are commonly first derived in their principal axis system (PAS), in which the tensor is diagonal, and rotated to the LAB frame using Wigner rotation matrices of 2nd rank ($\mathcal{D}^{(2)}_{nm}$).[6] For a single rotation from the PAS to the LAB frame, the tensor rotation operation is represented by a sum of 2nd rank Wigner matrix components and three Euler angles (Ω^{PL}: α_{PL}, β_{PL}, γ_{PL}) between the two frames.

$$V^{(LAB)}_{20} = \sum_{m=-2}^{2} V^{(PAS)}_{2m} \mathcal{D}^{(2)}_{m0}(\Omega_{PL}) \tag{1}$$

Euler rotations in this study use the Rose Z-Y-Z convention.[7] We use the simplified notation of $\mathcal{D}^{(2)}_{m0}(\Omega_{PL}) \equiv \mathcal{D}^{PL}_{m0}$ in the following equations.

The PAS frame is defined by the local geometry of the interaction. For example, the principal component, $V^{(PAS)}_{20}$, or anisotropy of the dipolar tensor, is collinear with the vector connecting the two dipolar spins, and this tensor is axially symmetric in the absence of local motion (i.e. $V^{(PAS)}_{2\pm2} = 0$). Consequently, the asymmetry of the tensor is zero, where the asymmetry is defined as follows.[6]

$$\eta^{(PAS)} = \frac{V^{(PAS)}_{22} + V^{(PAS)}_{2-2}}{V^{(PAS)}_{20}} \tag{2}$$

The CSA tensor principal component for a backbone carbonyl in a protein is orthogonal to the OCN plane and axially asymmetric ($\eta \neq 0$).[8]

By virtue of the fact that molecules are fixed in place by the crystalline lattice in solid samples, solid-state NMR can measure the orientation dependence and shape (anisotropy and asymmetry) of the 2nd rank spatial tensor as well as its local orientation to other interaction tensors and molecular groups. The 2nd rank tensor contains rich information on the local orientations and distances between nuclei from the dipolar tensor, and the orientation and distribution of the electron density at a nucleus from the

chemical shift tensor.[9] In the solution state, molecules tumble isotropically such that the time and ensemble average of the 2nd rank component, $V_{20}^{(LAB)}$, is equal to zero, and this information is lost from the spectrum—though they can be indirectly recaptured from 2nd order Hamiltonian terms and relaxation.[10] The anisotropic magnetic interactions can be directly reintroduced in the solution-state spectrum with PA, using either liquid crystals or magnetically-induced molecular alignment.[11] PA offers the opportunity to measure small deviations in frequencies originating from RDCs and RACSs (see **Table 1** for definitions), and these can then be correlated to information on molecular geometry, like bond orientations in a molecule.[12] In PA samples, molecules are uniaxially aligned, thereby losing useful information on the 2nd rank tensor. RDCs produce information analogous to solid-state NMR measurements of membrane proteins experiencing uniaxial diffusion in membranes. PRO samples in crystalline hydrogels, by contrast, report on the orientation dependence of the magnetic orientation tensor without losing information from PA. The key difference, as discussed below, is that PRO samples contain more complete information on the spatial tensor at the cost of information on the orientation of the magnetic interaction in the molecular frame. Consequently, information gathered from PRO and PA samples are complementary.

Table 1. Symbols, abbreviations and definitions

Symbol	Abbreviation and Definition
-	**PRO**. Partially randomly oriented
-	**PA**. Partially aligned
D_{ij}	**RDC**. Residual dipolar coupling between spins 'i' and 'j' from a PA sample.
δ_{ij}	**RDA**. Residual dipolar anisotropy between spins 'i' and 'j.' The RDA is directly measured from a PRO sample.
η_{ij}	Residual dipolar asymmetry between spins 'i' and 'j' measured from a PRO sample.
C_i	**RACS**. Residual anisotropic chemical shift for spin 'i' from a PA sample.[8] The RACS is sometimes referred to as the RCSA in the liquid crystalline NMR literature.

$\Delta\delta_i$	**RCSA**. Residual chemical shift anisotropy for spin 'i.' The RCSA is directly measured from a PRO sample.
δ_i	**RRCSA**. Residual reduced chemical shift anisotropy[9] measured from a PRO sample. $\delta_i = \frac{2}{3}\Delta\delta_i$
η_i	Residual chemical shift asymmetry for spin 'i' measured from a PRO sample.
-	**RQS**. Residual quadrupolar splitting from a PA sample.
-	**RQA**. Residual quadrupolar anisotropy, from a PRO sample.

In the following sections, we will derive the theory for PA samples with uniaxial and biaxial alignment as well as randomly oriented samples with uniaxial powder patterns and biaxial powder patterns. The hdNMR PRO samples described here are consistent with biaxial powder patterns.

Uniaxial partial alignment. The spherical tensor representing the spatial component of the dipolar Hamiltonian in the LAB frame, $V_{20}^{(LAB)}$, can be written in terms of the components in its PAS, $V_{20}^{(PAS)}$, using Wigner rotation matrices of second rank.[6] For a biomolecule dissolved in an aligned nematic liquid crystal, the transformation is conducted from the PAS to a common frame in the molecule, $\mathcal{D}_{0m}^{PM}$, then from the molecular frame to the orientation(s) of interaction with the liquid crystal (CRYS), $\mathcal{D}_{mn}^{MC}(i)$, and finally transformed from the liquid crystal to the laboratory frame, $\mathcal{D}_{n0}^{CL}$.

$$V_{20}^{(LAB)} = \sum_i^N p_i \sum_{m,n} V_{20}^{(PAS)} \mathcal{D}_{0m}^{PM} \mathcal{D}_{mn}^{MC}(i) \mathcal{D}_{n0}^{CL} \tag{3}$$

For simplicity, we have used an axially symmetric PAS tensor representative of a dipolar tensor in the absence of rapid motion; the q=±2, ±1 components of the axially symmetric $V_{2q}^{(PAS)}$ tensor are zero. The biomolecule may interact with the liquid crystal with multiple distinct interaction orientations, N, each with a population, p_i. The sum of the populations is the degree of alignment—typically on the order of 10^{-3} for biomolecules partially oriented with a liquid crystal by NMR. For a dipolar interaction,

the spatial tensor dipolar anisotropy ($V_{20}^{(PAS)}$) depends on the gyromagnetic ratios of the two spins (γ_i and γ_j), the distance between the spins (r_{ij}), Planck's constant ($\hbar$, in radial units) and the vacuum permittivity (μ_0).

$$\omega_{ij} = -\frac{\mu_0 \hbar \gamma_i \gamma_j}{4\pi r_{ij}^3} \tag{4}$$

The liquid crystal samples used for measuring RDCs are uniaxially aligned with n=0.

$$V_{20}^{(LAB)} = \sum_i^N p_i \sum_m V_{20}^{(PAS)} \mathcal{D}_{0m}^{PM} \mathcal{D}_{m0}^{MC}(i) \left\langle d_{00}^{CL} \right\rangle \tag{5}$$

Uniaxial ordering occurs due to diffusion of the molecule about the crystalline director, rapid diffusion of the liquid crystal directors about the magnetic field, or both effects together. In general, the liquid crystal director forms an angle β, depending on the diamagnetic susceptibility of the liquid crystal, with respect to the magnetic field. Uniaxial orderering results in the averaging of the n=$\pm$2 and $\pm$1 components to zero. The $\left\langle d_{00}^{CL} \right\rangle$ term represents the reduced Wigner component, and its time and ensemble average is the uniaxial liquid crystal order parameter, $S^{LC} = \left\langle P_2\left(\cos\beta_{CL}\right) \right\rangle$, where P_2 is the second Legendre polynomial.

In the simplest case, the molecule interacts with the liquid crystal with a single invariant angle, β_{MC}, made by the molecular z-axis and the crystal director. In this situation, equation (5) can be simplified for a single interaction orientation (N=1). If the transformation from the PAS, molecular and crystal frames remain time-independent, or time average independent (i.e. the motions are rapid enough to produce time-independent averages of the tensor components), then the Wigner closure theorem[6] further simplifies the expression.

$$V_{20}^{(LAB)} = pV_{20}^{(PAS)}d_{00}^{PC}S^{LC} \tag{6}$$

In the more general case, the molecule interacts with the liquid crystal with multiple orientations (N>1), and equation (5) produces a weighted average of the $p_i\mathcal{D}_{m0}^{MC}(i)$ Wigner matrix components.

$$V_{20}^{(LAB)} = S^{LC}\sum_m V_{20}^{(PAS)}\mathcal{D}_{0m}^{PM}\left\langle \mathcal{D}_{m0}^{MC}\right\rangle \tag{7}$$

The RDC (D_{ij}) between spins 'i' and 'j' corresponds to the $V_{20}^{(LAB)}$ tensor component, and the usual RDC equation is derived.[13]

$$D_{ij} = S^{LC}\sum_m V_{20}^{(PAS)}\mathcal{D}_{0m}^{PM}\left\langle \mathcal{D}_{m0}^{MC}\right\rangle \tag{8}$$

$$D_{ij} = \left(D_{a,\max}/2\right)S^{LC}\left(3\cos^2\theta - 1 - \eta_A\sin^2\theta\cos2\varphi\right) \tag{9}$$

The angles θ and φ represent the polar and azimuthal angles between the PAS and the molecular alignment frame. The $D_{a,max}$ is equal to $V_{20}^{(PAS)}\mathcal{D}_{00}^{PM}\left\langle \mathcal{D}_{00}^{MC}\right\rangle$ and $\eta_A = -\sqrt{6}\eta$. These are the alignment tensor anisotropy and asymmetry parameters. In the case that the molecule interacts with the liquid crystal with only one orientation, as described in equation (6), the alignment asymmetry is equal to 0. Note that this situation also arises when the molecular frame has a 3-fold or higher symmetry axis and the populations of these orientations are the same, such that the m=±2 and ±1 components average to zero.

Biaxial partial alignment. Biaxial liquid crystals may align along two axes instead of one.[4] To our knowledge, aqueous biaxial liquid crystals suitable for measuring biomolecular RDCs, RACSs and residual quadrupolar splittings (RQSs) have not been found. However, useful developments in combining multiple uniaxial alignment media hold promise for introducing alignment along multiple axes.[14]

Aligned biaxial liquid crystals differ from uniaxial liquid crystals in the uniaxial ordering in equation (5). The orientations between the CRYS frame and the LAB frame (α^{CL}, β^{CL}) are either fixed or their average remains time independent. Consequently, instead of a single liquid crystal order parameter, there are now five (S_n^{LC}, with n=±2, ±1, 0).

$$V_{20}^{(LAB)} = \sum_i^N p_i \sum_{m,n} V_{20}^{(PAS)} \mathcal{D}_{0m}^{PM} \mathcal{D}_{mn}^{MC}(i) S_n^{LC} \qquad (10)$$

In contrast to the biaxial powder patterns discussed below, the biaxial order parameters in biaxial liquid crystalline samples are simply numbers between -0.5 and 1.0, and they are uniform throughout the sample.

Equation (7) can be modified for biaxial alignment.

$$V_{20}^{(LAB)} = \sum_{m,n} V_{20}^{(PAS)} \mathcal{D}_{0m}^{PM} \left\langle \mathcal{D}_{m0}^{MC} \right\rangle S_n^{LC} \qquad (11)$$

Likewise, the RDC (D_{ij}) between spins 'i' and 'j' corresponds to the $V_{20}^{(LAB)}$ tensor component.

$$D_{ij} = \sum_{m,n} V_{20}^{(PAS)} \mathcal{D}_{0m}^{PM} \left\langle \mathcal{D}_{mn}^{MC} \right\rangle S_n^{LC} \qquad (12)$$

Biaxial order parameters can be grouped into two parameters:[15] a liquid crystal order parameter, S_0^{LC}, and a biaxial asymmetry parameter, $\eta_{LC} = S_2^{LC} + S_{-2}^{LC}$. The solution to equation (12) has many terms, but the final expression has only one value for the RDC of each spin pair, like equation (9). Equation (12) is simplified to equation (8) when the biaxial asymmetry parameter is zero (i.e. a uniaxial phase).

Fully aligned biaxial liquid crystals offer RDC information analogous to uniaxial liquid crystal systems. The interesting difference between the two types of liquid crystals

is the possibility of changing the biaxial asymmetry parameter of a sample. In principal, a change in the sample composition or the application of an electric field orthogonal to the magnetic field may change the biaxial asymmetry, thus offering new information unavailable from a single RDC dataset in a uniaxial liquid crystal.

In practice, fully aligned biaxial liquid crystals are difficult to achieve in a magnetic field.[15] Biaxial liquid crystals may order along the polar angle, β^{CL}, and remain statically disordered along the azimuthal angle, α^{CL}. For an axially symmetric tensor in the PAS, the spectra will manifest only a single coupling, regardless of the ordering in the α_{CL} angle. A ^2H spin, for example, with an axially symmetric quadrupolar tensor will always show a doublet in a biaxial liquid crystal (see Figure S1 in Supplementary Information). For an axially asymmetric tensor, static disorder about the azimuthal angle produces powder lineshapes that do not appear as Pake doublets (Figure S1).

Uniaxial powder patterns. For a constrained liquid crystal sample with uniaxial diffusion, the director orientation β_{CL} may be statically distributed randomly over a sphere, thus modulating the uniaxial liquid crystal order parameter $S^{LC} = \left\langle P_2\left(\cos\beta_{CL}\right)\right\rangle$. This situation arises in the solid state for a membrane protein subject to director axis diffusion in a randomly oriented membrane.[16] A *symmetric* powder pattern results from a uniaxial powder pattern. In the case of a powder pattern formed from randomly distributed crystal orientations with uniaxial alignment, the measured anisotropy is proportional to the RDC.

$$
\begin{aligned}
D_{ij}(\beta) &= \left(D_{a,\max}/2\right)\left(3\cos^2\theta - 1 - \eta_A \sin^2\theta\cos 2\varphi\right)\left(\tfrac{1}{2}(3\cos^2\beta - 1)\right) \\
&= (D_{ij}/S^{LC})\left(\tfrac{1}{2}(3\cos^2\beta - 1)\right)
\end{aligned}
\tag{13}
$$

In this situation, no new information is gained from the uniaxially aligned powder pattern in comparison to the uniaxially PA sample.

Partially randomly oriented samples and biaxial powder patterns. As demonstrated in the Results and Discussion, the PRO crystalline hydrogel samples described in this manuscript are different because they appear to not experience uniaxial ordering. The samples produce biaxial powder patterns analogous to powder samples in the solid-state.

The key difference in the theory arises in equation (3), as the n=±2 and n=±1 do not average to zero. The time dependence of the uniaxial diffusion requires that the transformation between the CRYS and LAB frames must be done separately in equation (5). In PRO samples, this transformation is time independent, or time-average independent, because the crystal directors are fixed in place by the hydrogel.

$$V_{20}^{(LAB)} = \sum_{i}^{N} p_i \sum_{m} V_{20}^{(PAS)} \mathcal{D}_{0m}^{PA}(i) \mathcal{D}_{m0}^{AL} \tag{14}$$

We have introduced a motionally averaged frame (AVE), which describes the effect of rapid whole body, segmental or internal motions on the $V_{20}^{(PAS)}$ tensor. In the absence of rapid molecular motion, the AVE tensor is simply equal to the PAS tensor.

Equation (14) has made use of the Wigner closure theorem to simplify the transformations between AVE, CRYS and LAB frames. In the situation when these transformations are time-average independent, as found for the samples in this study and the subsequent study, their transformation can be simplified.

$$\mathcal{D}_{m0}^{AL} = \sum_{w} \mathcal{D}_{mw}^{AC} \mathcal{D}_{w0}^{CL} \tag{15}$$

The new Ω_{AL} angles, like the Ω_{CL} angles, are randomly distributed over a sphere.

The molecule's interaction orientations (p_i) with the crystal can be recast as part of the transformation between the PAS and the AVE frame. The different interaction orientations are equivalent to an N-site hop of the whole molecule. Thereafter, the transformation between the average frame and the laboratory frame can be conducted.

$$V_{20}^{(LAB)} = \sum_m V_{20}^{(PAS)} \left\langle \mathcal{D}_{0m}^{PA} \right\rangle \mathcal{D}_{m0}^{AL} \tag{16}$$

The powder pattern generated by fixing the crystal orientations in the hydrogel matrix are summed over the five $\mathcal{D}_{m0}^{AL}$ components, thus representing a biaxial powder pattern.

In PRO samples, the residual dipolar anisotropy (RDA, δ_{ij}) and residual dipolar asymmetry (η_{ij}) of the motionally averaged tensor can be collected separately in the powder pattern spectra. The RDA and η_{ij} are defined as follows:

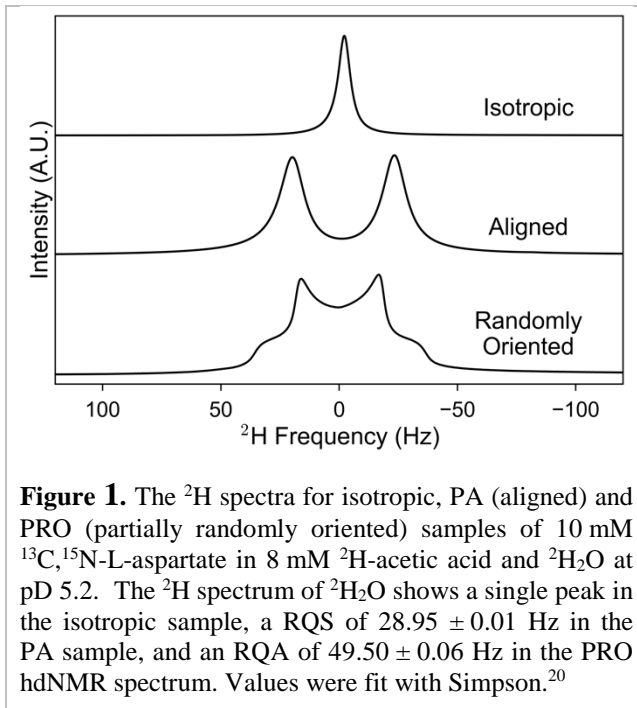$$\delta_{ij} = V_{20}^{(PAS)} \left\langle \mathcal{D}_{00}^{PA} \right\rangle \tag{17}$$

$$\eta_{ij} = \left(V_{20}^{(PAS)} \left\langle \mathcal{D}_{02}^{PA} \right\rangle + V_{20}^{(PAS)} \left\langle \mathcal{D}_{0-2}^{PA} \right\rangle \right) / \delta_{ij} \tag{18}$$

The CSA and quadrupolar interactions have a residual chemical shift anisotropy (RCSA, $\Delta\delta_i$) and residual quadrupolar anisotropy (RQA), respectively.

RESULTS

The ^2H spectra for ^2H_2O in $^{13}C,^{15}N$-L-aspartate samples are presented in Figure 1. The ^2H spectrum of the isotropic sample shows a single resonance in which isotropic tumbling of the ^2H_2O molecules collapses the quadrupolar coupling to a single peak. This is due to isotropic averaging of the 2nd rank spatial term to a value of zero, $\left\langle V_{20}^{(LAB)} \right\rangle = 0$. The PA sample is prepared with the addition of pinacyanol acetate (PNA) liquid crystal, which aligns spontaneously in the magnetic field[17,18] and produces a doublet with a net

residual quadrupolar splitting (RQS). Addition of molten agarose to the PNA sample, followed by vortexing and slow annealing to form a crystalline hydrogel matrix, produces a PRO hdNMR sample with the crystal director orientations distributed randomly in a spherical pattern. Molecules in solution interact weakly with the randomly oriented crystals, and the ^{2}H spectrum for the ^{2}H$_2$O resonance of this sample represents a PRO Pake pattern, analogous to the solid-state NMR powder pattern.[6] The PRO hdNMR spectrum is not even about the central frequency, likely due to small concentration gradients of the liquid crystal in the sample,[19] yet it is accurately fit to a quadrupolar powder spectrum.
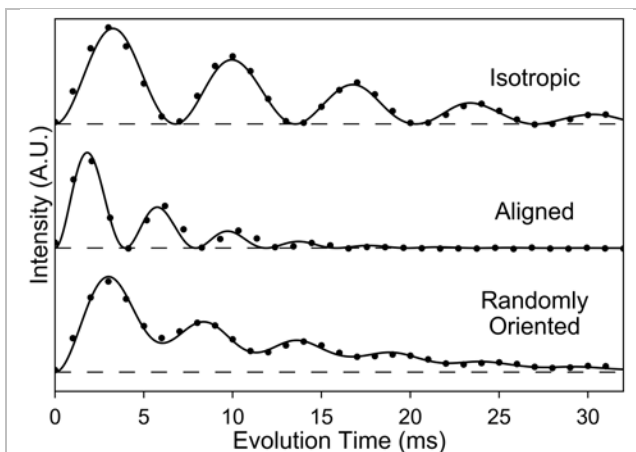

Figure 1. The ^{2}H spectra for isotropic, PA (aligned) and PRO (partially randomly oriented) samples of 10 mM ^{13}C,^{15}N-L-aspartate in 8 mM ^{2}H-acetic acid and ^{2}H$_2$O at pD 5.2. The ^{2}H spectrum of ^{2}H$_2$O shows a single peak in the isotropic sample, a RQS of 28.95 ± 0.01 Hz in the PA sample, and an RQA of 49.50 ± 0.06 Hz in the PRO hdNMR spectrum. Values were fit with Simpson.[20]

The ^{2}H PRO spectrum is consistent with a rapid exchange of ^{2}H$_2$O molecules between an isotropic state (99.962%) and a bound state to the PNA crystallites (0.037%). Water molecules maintain the same residual orientation throughout the evolution of the experiment, and they do not appear to diffuse appreciably between different crystal orientations, which would significantly broaden the spectrum in an orientation-dependent manner. Consequently, the spectrum represents a spherically distributed sum of different crystal orientations. Since water molecules diffuse more rapidly than the other molecules in this study, we predict and observe that

larger molecules also preserve the local orientation information throughout the evolution of the FID.

We achieved high-resolution and site-specific measurements of anisotropic dipolar and CSA tensors in ^{13}C,^{15}N-L-aspartate using SLF NMR pulse sequences. SLF pulse sequences are the same as their non-SLF counterparts, except the heteronuclear spin Insensitive Nuclei Enhanced Polarization Transfer (INEPT) periods are evolved together in their own dimensions (Figure S2). The forward and reverse INEPT periods are evolved together to avoid emphasizing only a subset of crystal orientations. The SLF variant of a ^{13}C heteronuclear single quantum coherence (SLF-^{13}C-HSQC) pulse sequence effectively measures the dipolar and CSA powder patterns in PRO samples.

Figure 2 shows the $\{^1H^\alpha$-$^{13}C^\alpha\}$ 1D projection from the INEPT evolution period of the ^{13}C-SLF-HSQC 3D spectrum. The data were collected from the $^{13}C^\alpha$ peak for the isotropic, PA and PRO samples of ^{13}C,^{15}N-L-aspartate. In a typical HSQC, the J_{CH}-coupling is nearly the same for all spin pairs in an isotropically tumbling molecule, and the INEPT period is fixed to a value near the average transfer time, $J^{-1}/2$ (total INEPT time), for maximum transfer of antiphase magnetization.[1]

Figure 2. Isotropic, PA (aligned) and PRO (randomly oriented) 1D projections of the $\{^1H$-$^{13}C\}$ dimension in a SLF-^{13}C-HSQC spectrum for 10 mM ^{13}C,^{15}N-L-aspartate in 8 mM ^{2}H-acetic acid and ^2H_2O at pD 5.2. The time evolution for the ^{13}C,^{15}N-L-aspartate $\{^1H^\alpha$-$^{13}C^\alpha\}$ INEPT dimension is shown for the $^{13}C^\alpha$ peak. Experimental points are shown in filled circles with the best-fit simulation drawn as a solid line. Simulations conducted using Simpson.[21] The isotropic sample oscillates with a J_{CH}-coupling of 144.39 ± 0.03 Hz (lb = 9.6 Hz). The PA $^1H^\alpha$-$^{13}C^\alpha$ RDC D_{CH} = -190.91 $\pm$ 0.05 Hz (lb = 40.6 Hz). The PRO $^1H^\alpha$-$^{13}C^\alpha$ RDA δ_{CH} = -38.6 $\pm$ 0.1 Hz (lb = 12.1 Hz). Traces have been normalized to the maximum intensity.

Evolving this coupling in the $\{^1H^\alpha\text{-}^{13}C^\alpha\}$ INEPT dimension for the isotropic samples shows an oscillation at a single frequency of J_{CH} (in Hz) with an intensity modulation of $\sin^2(\pi J_{CH}t)$. In the PA sample, the J_{CH}-coupling is further increased or decreased by the RDC (D_{CH}-coupling). Since aligned samples have only a single RDC for every spin pair, the INEPT period oscillates at a single frequency of $D_{CH}+J_{CH}$, and the oscillation reaches zero intensity at multiples of $t=1/(D_{CH}+J_{CH})$. The RDC, D_{ij}, contains information on the orientation of the dipolar coupling in the molecular frame for bonded nuclei.[12] If the RDC is large enough, varying the INEPT duration may be needed for the effective transfer of magnetization between spins in an HSQC.[22]

In PRO samples, SLF pulse sequences are used to measure the powder distribution of dipolar couplings and their frequencies. The $\{^1H^\alpha\text{-}^{13}C^\alpha\}$ INEPT dimension of the SLF-^{13}C -HSQC for the PRO sample evolves as a distribution of $J_{CH}+D_{CH}$-coupling frequencies, where the dipolar couplings vary in sign and magnitude from the different orientations of the crystals as described in equation (16). As a result, the $\{^1H^\alpha\text{-}^{13}C^\alpha\}$ dimension represents a spherically-weighted sum of a distribution of frequencies, producing an intensity offset proportional to the $^1H^\alpha\text{-}^{13}C^\alpha$ RDA, δ_{CH}, of the tensor (equation (17)). The RDA and the dipolar tensor asymmetry (equation (18)) contain information on the bond length as well as the total dynamics on a millisecond timescale for the $H^\alpha\text{-}C^\alpha$ bond.

These experiments were extended to additional dimensions and correlated to high-resolution chemical shift dimensions. We collected an SLF-HA(CA)CO 3D spectrum and simulated this spectrum using Simpson[21] to correlate the orientation of the $^1H^\alpha\text{-}^{13}C^\alpha$ dipolar tensor to the ^{13}C' CSA tensor. A comparison of this experiment for isotropic and PRO samples is presented in Figure 3.

The isotropic and PRO samples have comparable linewidths in the ^{1}H dimension (Figure 3A), consistent with the very weak interaction between L-aspartate molecules and the PNA crystals in the PRO samples. The ^{1}H$^\alpha$ linewidths are 23.5 Hz and 20.5 Hz for the isotropic and PRO samples, respectively. In the isotropic and PRO samples, the unresolved 3-bond $J_{H\alpha H\beta}$-coupling of 6-8 Hz[23] contributes a cosine modulation that increases this linewidth. The ^{1}H$^\alpha$ linewidth in the PRO sample is additionally modulated by the ^{1}H$^\alpha$ RCSA and ^{1}H-^{1}H $\delta_{H\alpha H\beta}$ RDA powder distributions. The former is expected to broaden the peak, while

Figure 3. The SLF-HA(CA)CO spectrum for the isotropic and PRO samples of ^{13}C,^{15}N-L-aspartate at pD 5.2 in ^{2}H$_2$O. (**A**) The 1D projection of the ^{1}H$^\alpha$ peak for the isotropic aspartate sample and the PRO hdNMR sample. The ^{1}H linewidths for the isotropic and PRO peaks are 23.5 Hz and 20.5 Hz, respectively. (**B**) The {^{1}H$^\alpha$-^{13}C$^\alpha$}/^{13}C' 2D projection for the isotropic sample. (**C**) The {^{1}H$^\alpha$-^{13}C$^\alpha$}/^{13}C' 2D projection for the PRO sample. The best-fit values are δ_{CH} = -31.4 ± 0.1 Hz, $\delta_{C'}$ = -11.04 ± 0.03 Hz (-63.5 ± 0.2 ppm), $\eta_{C'}$ = 0.50 ± 0.01, β_{AC} = 2.0 ± 0.2° and γ_{AC} = -44.2 ± 2.3° or 135.4 ± 1.8°. Fits that included a dipolar asymmetry parameter, η_{CH}, did not statistically improve the quality of the fit, according to an F-test (α<0.05). The PRO sample for these spectra was different from the sample in Figure 2.

the latter is expected to narrow the peak. Altogether, the PRO ^{1}H$^\alpha$ linewidth is narrower than the isotropic linewidth because the negative sign of the ^{1}H-^{1}H RDA (equation (4)) subtracts from the positive $J_{H\alpha H\beta}$-coupling and reduces the net $J_{H\alpha H\beta}+\delta_{H\alpha H\beta}$ coupling. The
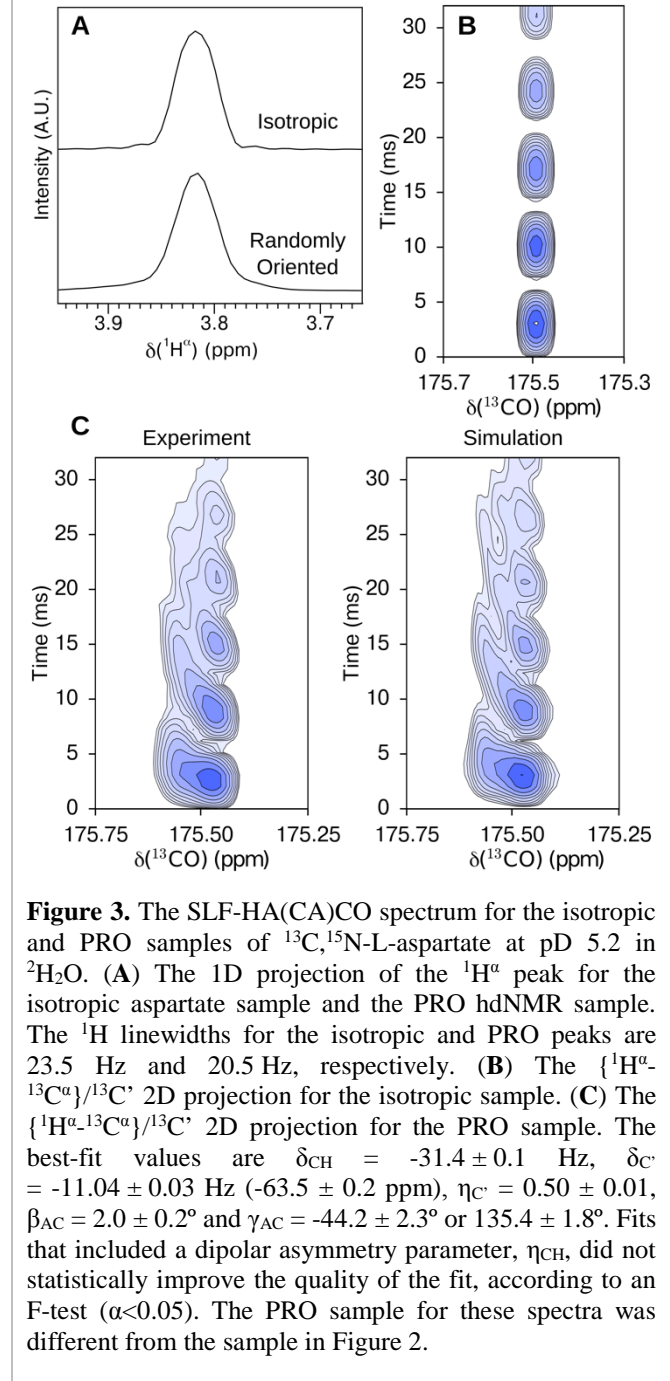
contribution of the RDA is manifested as a powder pattern with a distribution of dipolar frequencies between $\delta_{H\alpha H\beta}$ and $-0.5\delta_{H\alpha H\beta}$.

The $\{^1H^\alpha-^{13}C^\alpha\}/^{13}C'$ 2D projection of the SLF-HA(CA)CO spectrum shows clear differences between the isotropic and PRO samples. The isotropic $^{13}C,^{15}N$-L-aspartate sample (Figure 3B) shows a single $^{13}C'$ peak in the ^{13}C dimension, which oscillates at a frequency of the J_{CH}-coupling in the $\{^1H^\alpha-^{13}C^\alpha\}$ dimension. The 2D projection for the PRO $^{13}C,^{15}N$-L-aspartate sample (Figure 3C) represents a spherical distribution of $^{13}C'$ CSA orientations in the ^{13}C dimension and $^1H^\alpha-^{13}C^\alpha$ dipolar orientations in the $\{^1H^\alpha-^{13}C^\alpha\}$ dimension. The dipolar and CSA tensors maintain a fixed relative orientation in the molecule, producing a distribution of frequencies in the powder pattern that are correlated. Consequently, the spectra show a twisting oscillation between the $^1H^\alpha-^{13}C^\alpha$ dipolar and $^{13}C'$ CSA tensor dimensions. These coupled frequencies contain detailed information on the relative orientation of the $^1H^\alpha-^{13}C^\alpha$ dipolar and $^{13}C'$ CSA tensors.

We used statistical F-tests ($\alpha<0.05$) to find that the $^1H^\alpha-^{13}C^\alpha$ RDA (δ_{CH}), $^{13}C'$ RCSA ($\delta_{C'}$), $^{13}C'$ chemical shift asymmetry ($\eta_{C'}$) and relative orientation (β and γ, relative to the dipolar PAS) were the minimum number of parameters needed to fit the spectrum. The measurement of an axially asymmetric CSA tensor ($\eta_{C'} = 0.50 \pm 0.01$) is consistent with the random distribution of crystallite orientations and a biaxial powder pattern (see Figure S3 and S4).

The dipolar $\{^1H^\alpha-^{13}C^\alpha\}$ dimension is accurately fit to an axially symmetric dipolar tensor, which is consistent with only a single orientation of interaction between aspartate and the PNA crystallites (N=1, equation (14)). Using a static $^1H-^{13}C$ dipolar coupling of -22.7kHz for a bond length of 1.1Å, the population of the isotropic (99.86%) and bound (0.14%) states of L-aspartate can be determined. Accordingly, the $^1H-^{13}C$ RDA

can be used to directly calculate the $^{13}C'$ CSA tensor with very high precision (0.2ppm). The $^{13}C'$ CSA tensor $\delta_{C'}$ = -63.5 ± 0.2ppm and $\Delta\delta_{C'}$ = -95.2 ± 0.2 ppm. The $^{13}C'$ CSA tensor is axially asymmetric (η = 0.50 ± 0.01) with the δ_{11} component approximately collinear with the H^α-C^α bond, the COO plane orthogonal to the H^α-C^α dipole and the δ_{22}/δ_{33} components tilted away from the C^α-C' bond.
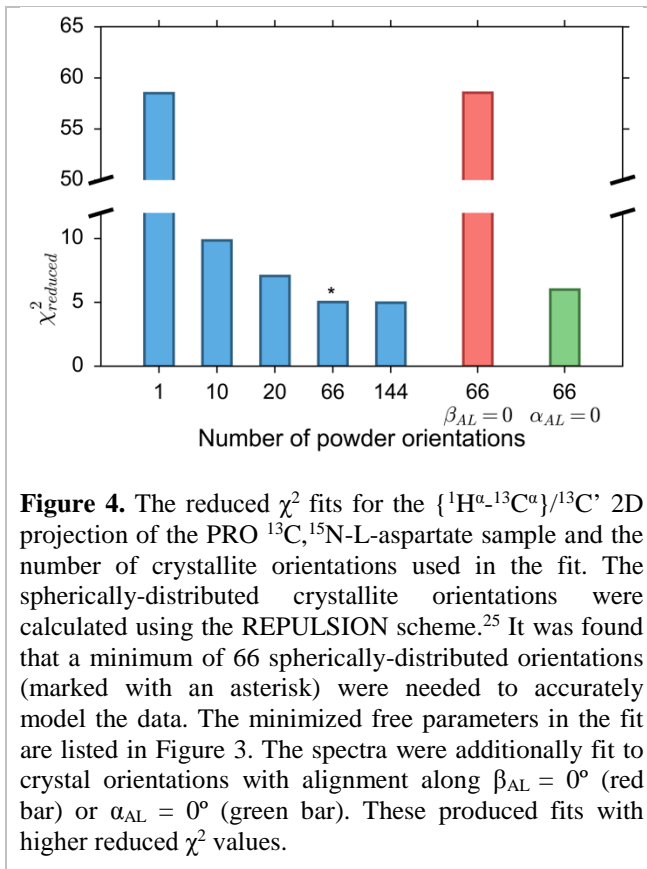
The CSA tensor parameters are 20-25% lower than values reported by solid-state NMR. The solid-state carboxylate $\delta_{C'}$ and $\eta_{C'}$ values are -79.3 ppm and 0.71 for a deprotonated carboxylate, and -83.6 ppm and 0.48 for a protonated carboxylic acid.[24] Our observed values are consistent with a deprotonated CSA tensor with a restricted rotational motion by *ca.* ±23° about the Cα-C' bond. In the solid-state, crystal packing interactions lock the carboxylate in place, producing a CSA tensor with a larger magnitude.

DISCUSSION

Comparison with uniaxially aligned and biaxially aligned samples. Uniaxially PA samples are commonly used for measuring RDCs, RACSs and RQSs by solution NMR, and they contain information on the orientation and length of bonds in a molecular frame.[12] Likewise, biaxial PA samples produce a single RDC for each spin pair or a single RACS or RQS for each nucleus, if the interaction tensor is axially symmetric or the liquid crystal is aligned along two axes. Biaxial liquid crystals may alternatively produce distorted powder lineshapes that do not resemble Pake patterns (Figure S1), if the interaction tensor is axially asymmetric and the biaxial liquid crystal is statically disordered along the second axis. None of these features are observed in the spectra collected for hdNMR PRO samples.

The crystalline hydrogel PRO samples in this study are different from uniaxial and biaxial PA samples because they show a *distribution* of dipolar, quadrupolar and

CSA values and a *single* Pake powder pattern, corresponding to the random distribution of crystallite orientations. The randomly oriented hdNMR ^{2}H Pake powder lineshape in Figure 1 shows a distribution of frequencies that are not consistent with uniaxial alignment and biaxial alignment. The ^{2}H$_2$O quadrupolar tensor is axially symmetric ($\eta \approx 0$) and can only produce a doublet spectrum for uniaxially and biaxially PA samples (Figure S1).

Figure 4. The reduced χ^2 fits for the {^{1}H$^\alpha$-^{13}C$^\alpha$}/^{13}C' 2D projection of the PRO ^{13}C,^{15}N-L-aspartate sample and the number of crystallite orientations used in the fit. The spherically-distributed crystallite orientations were calculated using the REPULSION scheme.[25] It was found that a minimum of 66 spherically-distributed orientations (marked with an asterisk) were needed to accurately model the data. The minimized free parameters in the fit are listed in Figure 3. The spectra were additionally fit to crystal orientations with alignment along $\beta_{AL} = 0°$ (red bar) or $\alpha_{AL} = 0°$ (green bar). These produced fits with higher reduced χ^2 values.

The randomly oriented spectrum in Figure 2 is also inconsistent with partial alignment because the oscillation in intensity does not reach zero after the initial point. In this spectrum, a distribution of dipolar couplings are evolving at the same time, producing a distribution in sin^2-waves. Likewise, a PRO sample and a distribution of dipolar and CSA frequencies produce the 'twisting' pattern for the randomly oriented {^{1}H$^\alpha$-^{13}C$^\alpha$}/^{13}C'

2D spectrum in Figure 3. The twisting pattern occurs as a result of the fixed geometry and correlated frequencies of the dipolar and CSA tensors.

The distribution in dipolar and CSA orientations is further exemplified in the χ^2 fits of the {^{1}H$^\alpha$-^{13}C$^\alpha$}/^{13}C' 2D spectrum (Figure 4). The spectrum is only accurately reproduced with at least 66 spherically-distributed orientations in the simulation ($\chi^2_{red} =$

5.0). A distribution aligned along β_{AL} and statically disordered along α_{AL}, which could arise in a partially aligned biaxial liquid crystal sample, also produces a statistically worse fit (Figure 4, red bar), according to an F-test ($\alpha<0.0001$).

Comparison with uniaxial powder pattern samples. Uniaxial powder patterns result from the rapid, uniaxial diffusion of the crystal director or from the molecule diffusing around the liquid crystal director. In uniaxial powder patterns, the crystal orientations are randomly distributed about the β_{AL} angle, but they are motionally averaged about the α_{AL} angle. The resulting powder patterns are *axially symmetric* and do not contain the full information of the anisotropic tensor.

The PRO samples described here do not represent uniaxial powder patterns: they are consistent with *biaxial* powder patterns and can be differentiated from uniaxial powder patterns in at least two different ways.

Characteristic 1: PRO samples may have axially asymmetric powder patterns ($\eta\neq0$), whereas uniaxial powder patterns are universally axially symmetric ($\eta=0$).

Characteristic 2: In uniaxial powder patterns, the RDA is linearly correlated to the RDCs for the same biomolecule in the same liquid crystal (without the hydrogel matrix). For a PRO sample, the RDA and RDC values are not linearly correlated because equation (9) is different from equation (17).

The first characteristic applies to our PRO L-aspartate sample in this study.

The $^{13}C'$ CSA of aspartate is axially asymmetric ($\eta_{C'} = 0.50 \pm 0.01$, Figure 3) in our PRO crystalline hydrogel samples, which is inconsistent with a uniaxial powder pattern. A uniaxial powder pattern distribution also does not fit the data accurately

(Figure 4 and Figures S3 and S4). The averaging of crystal orientations about the azimuthal angle ($\alpha_{AL} = 0°$) produced substantially worse fits, as evaluated by an F-test ($\alpha < 0.01$).

Distribution of crystallite orientations. The liquid crystals are relatively low in density in aqueous solution, compared to a crystalline solid-state sample, and the crystal director orientations may be fixed in place by the hydrogel in a spherical, yet non-uniform distribution. A non-uniform distribution can be avoided by reprocessing samples, as described in the Experimental Section. The uniform distribution of crystallites can be evaluated from the powder lineshape of the ^2H_2O resonance for the sample.

The ^2H Pake patterns demonstrate that our PRO samples are uniformly and randomly distributed in their β_{AL} angles. Since the ^2H quadrupolar coupling of ^2H_2O is nearly axially symmetric, the distribution of crystallites about the α_{AL} angle cannot be evaluated. However, fitting the axially asymmetric CSA tensor of the L-aspartate carboxylate reveals that our PRO samples are indeed distributed randomly in the α_{CL} angle.

Yet the possibility remains that the α_{CL} angles are distributed non-uniformly. A non-uniform distribution in α_{CL} would skew the measured asymmetry ($\eta_{C'}$) for the $^{13}C'$ CSA tensor and impact the azimuthal angle between the average frame and the crystal frame (α_{AC}). However, the accuracy of the fit RDA and RCSA parameters would remain unaffected.

Another possibility that would impact the accuracy of PRO tensor data is movement of the crystallites within the hydrogel matrix. The crystal orientations, and the α_{AL} and β_{AL} angles, are highly constrained, as evidenced by the Pake patterns measured for ^2H_2O and aspartate. Rapid, small amplitude motions could still impact the powder

summation terms, $\mathcal{D}_{m0}^{AL}$, in equation (16) by reducing their magnitudes with a motional order parameter, S_m^{AL}. If the crystal motion is uniform about all axes, such that $S_m^{AL} = S^{AL}$ for m=±2, ±1 and 0, then the crystal motion order parameter would simply scale the degree of alignment (p_i) and the rest of the analysis would remain unchanged. If the crystal motion is non-uniform about the different axes, such that the S_m^{AL} order parameters are different, then the fit anisotropies and asymmetries would be scaled differently. This scaling could change the measured asymmetry parameters. However, this scaling should not impact the relative RDA, RCSA and RQA values ($V_{20}^{(AVE)}$), as these would all be scaled uniformly throughout the sample.

In the above analysis, we have found that the RDA, RCSA and RQA values can be precisely determined from PRO samples. The possibility of a non-uniform distribution in α_{AL} or small amplitude motions in the crystal orientations may introduce inaccuracies in the measured powder lineshape asymmetries. However, a symmetric tensor cannot be made to appear asymmetric from non-uniform α_{AL} distribution, if the α_{AL} and β_{AL} angles are not correlated (see Distribution of crystal orientations and symmetric tensors in the Supplementary Information). We are currently investigating alternative approaches to characterizing these orientations by measuring powder lineshapes in a goniometer probe or with ^2H spins with axially asymmetric spatial tensors.

CONCLUSION

The hdNMR experiment offers new possibilities in accurately measuring and mapping the magnetic dipolar, CSA and quadrupolar interactions in molecules. These can be used to precisely refine the bond lengths, electron density distribution, dynamics and structure of molecules.

EXPERIMENTAL SECTION

Preparation of Pinacyanol acetate. Pinacyanol chloride (Santa Cruz Biotechnology) powder was added to silver acetate (Strem Chemicals) in a 1:2 molar ratio, vortexed for 30 seconds and dissolved in 100% ethanol (Decon Labs).[17] The solution was mixed in a 50-mL Falcon tube (Santa Cruz Biotechnology) on an orbital shaker for 5 minutes. The precipitated AgCl was filtered using a clearing column (Promega) and filter paper. The solution of PNA was lyophilized for 36 hours, and formation of the liquid crystal in water was confirmed by dissolving 15 mg/mL PNA in 20mM Tris pH 7.5 with 15% ^2H_2O and measuring the RQS by ^2H NMR. The measured RQS of the liquid crystal was 37.6 ± 1.9 Hz.

Preparation of partially randomly oriented crystalline hydrogel samples. The PNA sample was prepared by adding 8.7 mg PNA to 580 µL aqueous sample containing 15% ^2H_2O (15 mg/mL final concentration of PNA). The sample was mixed by repeating the following steps three times: vortex on a high setting for 1-2 minutes and incubate at 60ºC for 5 minutes. A solution of molten 20 mg/mL ultra-low melting temperature agarose (ULMPA, Sigma-Aldrich) at 60ºC was added to a final ULMPA concentration of 0.75-6 mg/mL. The mixture was vortexed at a high setting for 1 minute. The PNA-ULMPA sample mixture was annealed and equilibrated by placing the sample in a 37ºC shaker incubator (New Brunswick I-2500KC) for 30 minutes or longer, vortexing for 30 seconds and placing at 60ºC for 1 minute, then vortexing again for 30 seconds. The solution was transferred to a pre-heated NMR tube and stored at 60ºC for 20 minutes. Thereafter, the NMR tube was briefly vortexed, and the sample was collected to the bottom of the tube using a hand centrifuge. Samples were given 14-16 hours at room temperature to gel, and samples were kept at a temperature equal to 20-25ºC.

The spherical Pake distribution was measured from the RQA of ^2H_2O by ^2H NMR and successful gelation of the sample was confirmed by a PRO Pake spectrum that remained unchanged at 500-MHz (^1H Larmor frequency). The final concentration of ULMPA was optimized for each sample, using natural abundance samples, to produce a stable and unchanging Pake pattern. In the event that the ^2H spectrum was asymmetric and represented an inhomogeneous sample, the PRO sample was reprocessed by vortexing for 5 minutes followed by placing at 60°C for 10-15 minutes followed by brief vortexing and finally, using a hand centrifuge to settle the sample to the bottom of the NMR tube.

Preparation of the ^{13}C,^{15}N-L-aspartate partially aligned and partially randomly oriented samples. To prepare the PRO sample, we followed the procedure above by dissolving the PNA in a 10 mM ^{13}C,^{15}N-L-asparate solution (Cambridge Isotope Laboratories) in 8 mM ^2H-acetic acid (CIL) at pH 5.2 and 100 % ^2H_2O (Sigma Isotopes). The final concentrations of PNA and ULMPA were 15 and 0.75 mg/ml, respectively. The measured RQA of the sample was 47.15 ± 0.04 Hz. To prepare the PA sample, a 10 mM ^{13}C,^{15}N-L-asparate solution in 8 mM ^2H-acetic acid at pH 5.2 and 100 % ^2H_2O was added the 15 mg/ml PNA. The aligned RQS was 28.95 ± 0.01 Hz.

NMR Experiments. Experiments were collected on a Bruker Avance HD III 500-MHz NMR spectrometer equipped with a ^1H/^{13}C/^{15}N/^{31}P QXI room temperature probe with triple-axis gradients. All spectra were collected at 25.0°C, which was calibrated by measuring the chemical shift difference of the ^1H_3C and ^1HO resonances in a methanol standard, with an estimated precision of 0.1°C.[1]

Pake patterns were confirmed from ^2H NMR 1D spectra of the residual ^2H_2O peak as well as SLF spectra.

SLF spectra were collected by evolving the {^{1}H-^{13}C} INEPT periods in a separate dimension.[22] The SLF-^{13}C-HSQC was conducted on isotropic, PA and PRO ^{13}C,^{15}N-L-aspartate samples in ^{2}H$_2$O by evolving the {^{1}H-^{13}C} INEPT dimension and the ^{1}H direct dimension. See Figure S2 for a pulse sequence diagram of the SLF-^{13}C-HSQC. The {^{1}H-^{13}C} INEPT dimension was evolved with a 1.0 ms dwell period with 32 real points for a total acquisition time of 32.0 ms and processed without apodization.

The SLF spectra were collected by incrementing the {^{1}H-^{13}C} INEPT and {^{13}C-^{1}H} reverse INEPT delays together. Both INEPT periods were evolved together because keeping one of the INEPT periods with a fixed delay would introduce a selectivity filter for only a subset of orientations. However, since both INEPT periods evolve together, the detected magnetization is modulated by a $\sin^2$ intensity profile of the J- or J+D-coupling, instead of a sin-modulation in varying only one of the INEPT periods.

A SLF-HA(CA)CO 3D spectrum was collected on the PRO ^{13}C,^{15}N-L-aspartate sample as well as an isotropic ^{13}C,^{15}N-L-aspartate sample without liquid crystal and ULMPA. The {^{1}H-^{13}C} INEPT and reverse INEPT were evolved together in a separate dimension with a 1.0 ms dwell period and 32 real points for a total acquisition time of 32.0 ms. The ^{13}CO dimension was collected with a 1.989 ms dwell period with 128 complex States points for a total acquisition time of 254.6 ms. The ^{13}CO carrier frequency was 175 ppm.

The SLF-HA(CA)CO spectrum incorporates INEPT transfer periods between the ^{13}C$^\alpha$ and ^{13}C' nuclei. These INEPT transfer periods were kept constant with a total delay of 9.0ms, even though the J+D-coupling for the PRO samples represent a distribution of frequencies. However, it was assumed that the range for frequencies for this coupling—and other dipolar couplings for low-γ nuclei—is small in PRO samples, since the

estimated RDA $\delta_{13C\alpha-13C'}$ is *ca.* 3.6 Hz, based on the measured RDA $\delta_{1H13C\alpha}$ of -38.6 Hz. Consequently, the J+D-coupling only varies between *ca.* 53-59 Hz. In keeping the $^{13}C^{\alpha}$-$^{13}C'$ INEPT period fixed, we avoided the collection of an additional dimension in the experiment.

The SLF pulse sequences were collected without Rance-Kay (sensitivity enhanced) detection to minimize ^1H T_2 losses during the INEPT evolution periods. The $\{^1H-^{13}C\}$ INEPT and $^{13}C'$ dimensions were processed without apodization.

Simulations. Simpson (v4.1.1) simulations[21] were conducted on the University of Illinois at Chicago (UIC) Research Computing Cluster using 2 nodes with 16 Xeon E5-2670 CPUs and 128 GB of RAM each, running CentOS 6.5.

The ^2H spectra were fit with a REPULSION spherical distribution with 2000 orientations[25] using a single ^2H spin. The powder spectra are consistent with a single interaction orientation, as discussed in the Theory section. The reported RQA represents a scaled quadrupolar coupling by the degree of alignment, p.

$$RQC = p\frac{e^2Qq}{h} \tag{19}$$

The $\{^1H-^{13}C\}/^1H$ 2D projection for the ^{13}C-SLF-HSQC was conducted on isotropic, PA and PRO $^{13}C,^{15}N$-L-aspartate samples in ^2H_2O. The Simpson simulations used a $^1H^{\alpha}$, ^{13}C, $^1H^{\beta}$ and $^1H^{\beta}$ 4-spin system. The spectral parameters were optimized using the opt package in Simpson.[21] All Simpson simulations optimized the line broadening in each dimension and the Lorentzian-Gaussian ratio. Additionally, the isotropic simulation optimized the $J_{CH\alpha}$ and $J_{H\alpha H\beta}$ couplings. The best-fit values were $J_{CH\alpha} = 144.39 \pm 0.03$ Hz and $J_{H\alpha H\beta} = 8.69 \pm 0.03$ Hz. The J-couplings between the $^1H^{\alpha}$ and the two $^1H^{\beta}$ protons were treated the same. The value of the ^1H-^1H J-coupling, and

the ^{1}H-^{1}H dipolar couplings below, could be underestimated since they contribute a weak cosine-modulation to the INEPT evolution, which could be partially fit by the Gaussian contribution from the fit apodization function. Simpson v4.1 calculates the root mean square deviation (RMSD) to estimate the 95% confidence interval. We instead calculated and reported the 95% confidence interval from the χ^2 fit using the experimental noise, as previously described in the section on Chi-Square Fitting in Numerical Recipes in C.[26] The experimental noise in the spectrum was estimated using NMRPipe.[27]

The PA ^{13}C,^{15}N-L-aspartate simulation optimized the $^1D_{CH\alpha}$ and $^3D_{H\alpha H\beta}$ couplings. The optimized J-couplings from the isotropic refinement were used. The best-fit values for the RDCs were $D_{CH\alpha}$ = -190.91 $\pm$ 0.05 Hz and $D_{H\alpha H\beta}$ = 4.03 $\pm$ 0.05 Hz. The reported $^1H^\alpha$-$^1H^\beta$ RDC includes the motionally averaged $<r^{-3}>$ H^α-H^β distance as well as the order parameter between the H^α-H^β dipolar tensor.

The PRO ^{13}C,^{15}N-L-aspartate SLF-^{13}C-HSQC simulation optimized the $\delta_{CH\alpha}$ RDA and $\delta_{H\alpha H\beta}$ RDA principal components of the dipolar tensors. The optimized J-couplings from the isotropic refinement were used. The best-fit values for $\delta_{CH\alpha}$ and $\delta_{H\alpha H\beta}$ were -38.6 $\pm$ 0.1 Hz and -2.2 $\pm$ 0.1 Hz, respectively. The ^{2}H RQA for this sample was 47.16 $\pm$ 0.04 Hz. The PRO powder lineshape for the $^1H^\alpha$-$^{13}C^\alpha$ dipolar coupling was accurately fit to an axially symmetric tensor.

For the isotropic and PRO ^{13}C,^{15}N-L-aspartate samples, SLF-HA(CA)CO 3D spectra were collected. The 2-dimensional {^{1}H-^{13}C}/^{13}C' projection plane was extracted using the sum mode projection with NMRPipe[27] and refined using Simpson.[21] The spectrum was refined with 66 REPULSION orientations and a spin system with one ^{1}H and one ^{13}C nucleus. The $^1J_{CH}$-coupling of 144.4 Hz from an isotropic sample was used to refine the PRO sample. The RDA (δ_{CH}), the average dipolar coupling asymmetry (η_{CH}),

the reduced anisotropy of the $^{13}C'$ CSA tensor ($\delta_{C'}$), the asymmetry of the CSA tensor ($\eta_{C'}$), and the angles between the two tensors, β and γ, were refined. F-tests were conducted for each additional parameter included (Table S1), and it was found that all of these parameters, with the exception of η_{CH}, produced a statistically significant improvement in the fit ($\alpha<0.05$). Note that this was a different sample than the PRO $^{13}C,^{15}N$-L-aspartate sample used for the ^{13}C-SLF-HSQC experiment above.

AUTHOR INFORMATION

Corresponding author: justin@lorieau.com

ASSOCIATED CONTENTS

Supplementary Information. Description of the distribution of crystallite azimuthal angles and symmetric tensors; Table of the fit parameters for the SLF-HA(CA)CO spectrum; Plot for the simulated spectra of statically disordered biaxial aligned samples; Pulse sequence diagram for the SLF-^{13}C-HSQC; The χ^2 fit of the $^{13}C'$ RCSA tensor asymmetry from the SLF-HA(CA)CO spectrum; Plot of the comparison of the $\{^{1}H$-$^{13}C\}/13C'$ 2D projection for axially symmetric and asymmetric RCSA tensors.

REFERENCES

(1)   Cavanagh, J.; Fairbrother, W.; Palmer, A.; Skelton, N. *Protein NMR Spectroscopy: Principles and Practice*, 2nd ed.; Academic Press: Burlington, MA, 2007.

(2)   Tjandra, N.; Bax, A. *Science* **1997**, *278*, 1111–1114.

(3)   Luckhurst, G. R. *Thin Solid Films* **2006**, *509*, 36–48.

(4)   Luckhurst, G. R. *Thin Solid Films* **2001**, *393*, 40–52.

(5)   Steigel, A.; Spiess, H. W. *Dynamic NMR Spectroscopy*; Springer-Verlag: New York, 1978.

(6)   Schmidt-Rohr, K.; Spiess, H. *Multidimensional solid-state NMR and polymers*; Academic Press Inc.: San Diego, CA, 1994.

(7)   Rose, M. E. *Elementary Theory of Angular Momentum*; Dover Publications, Inc.: New York, NY, 1957.

(8)   Cisnetti, F.; Loth, K.; Pelupessy, P.; Bodenhausen, G. *ChemPhysChem* **2004**, *5*, 807–814.

(9)   Saitô, H.; Ando, I.; Ramamoorthy, A. *Prog. Nucl. Magn. Reson. Spectrosc.* **2010**, *57*, 181–228.

(10)   Goldman, M. *Quantum description of high-resolution NMR in liquids*; Oxford University Press: Oxford, 1988.

(11)   Bax, A. *Protein Sci.* **2003**, *12*, 1–16.

(12)   Bax, A.; Grishaev, A. *Curr. Opin. Struct. Biol.* **2005**, *15*, 563–570.

(13)   Torchia, D. A. *Prog. Nucl. Magn. Reson. Spectrosc.* **2015**, *84–85*, 14–32.

(14)   Ruan, K.; Tolman, J. R. *J. Am. Chem. Soc.* **2005**, *127*, 15032–15033.

(15)   Dong, R. Y. *Nuclear Magnetic Resonance of Liquid Crystals*; Partially Ordered Systems; Springer New York: New York, NY, 1997.

(16)   Lewis, B. A.; Harbison, G. S.; Herzfeld, J.; Griffin, R. G. *Biochemistry* **1985**, *24*, 4671–4679.

(17)   Thiagarajan-Rosenkranz, P.; Draney, A. W.; Smrt, S. T.; Lorieau, J. L. *J. Am. Chem. Soc.* **2015**, *137*, 11932–11934.

(18)   Rodríguez-Abreu, C.; Torres, C. A.; Tiddy, G. J. T. *Langmuir* **2011**, *27*, 3067–

3073.

(19) Ottiger, M.; Bax, A. *J. Biomol. NMR* **1998**, *12*, 361–372.

(20) Bak, M.; Rasmussen, J. T.; Nielsen, N. C. *J. Magn. Reson.* **2000**, *147*, 296–330.

(21) Tošner, Z.; Andersen, R.; Stevensson, B.; Edén, M.; Nielsen, N. C.; Vosegaard, T. *J. Magn. Reson.* **2014**, *246*, 79–93.

(22) Ward, J. M.; Skrynnikov, N. R. *J. Biomol. NMR* **2012**, *54*, 53–67.

(23) Bundi, A.; Wüthrich, K. *Biopolymers* **1979**, *18*, 285–297.

(24) Gu, Z.; McDermott, A. *J. Am. Chem. Soc.* **1993**, *115*, 4282–4285.

(25) Bak, M.; Nielsen, N. *J. Magn. Reson.* **1997**, *125*, 132–139.

(26) Press, W. H.; Teukolsky, S. A.; Vetterling, W. T.; Flannery, B. P. *Numerical recipes in C: The Art of Scientific Computing*, 2nd ed.; Cambridge University Press: New York, NY, 1992.

(27) Delaglio, F.; Grzesiek, S.; Vuister, G. W.; Zhu, G.; Pfeifer, J.; Bax, A. *J. Biomol. NMR* **1995**, *6*, 277–293.

TOC FIGURE